Resonance structure due to the $4d^{10}4f^7 \rightarrow 4d^9 4f^8$ transition in the photoionization cross section of atomic europium

Cheng Pan, Steven L. Carter, and Hugh P. Kelly
Department of Physics, University of Virginia, Charlottesville, Virginia 22901
(Received 5 April 1990)

Photoionization cross sections for the $4d$, $4f$, $5s$, $5p$, and $6s$ electrons and angular-distribution asymmetry parameters for the $4d$, $4f$, and $5p$ electrons of atomic europium at photon energies near the $4d^{10}4f^7 \rightarrow 4d^9 4f^8$ resonance have been calculated by use of many-body perturbation theory. Interactions among ionization channels were included in the calculation, and the results are compared with experiments and other calculations.

I. INTRODUCTION

Studies on the $4d^{10}4f^n \rightarrow 4d^9 4f^{n+1}$ resonance transition in the lanthanide elements ($Z=57$ to 71) were initiated by the observation of large peaks in the x-ray absorption spectra of lanthanide metals near the $4d$ absorption edge by Zimkina *et al.* in 1967.[1] Dehmer *et al.*[2] studied Coulomb interactions between the $4d$ and $4f$ electrons in these elements and attributed the peaks observed in the spectra to $4d^{10}4f^n \rightarrow 4d^9 4f^{n+1}$ transitions. Many experimental[3-11] and theoretical[12-20] studies have been reported. Photoionization cross sections have been calculated including electron correlations for the lanthanum,[14,15] cerium,[16] samarium,[20] europium (Eu),[17-20] and gadolinium[20] atoms.

The particularly strong $4d^{10}4f^n \rightarrow 4d^9 4f^{n+1}$ transitions in the lanthanide group of the rare-earth elements are related to orbital collapse phenomena due to potential barrier effects.[2,12,21-27] The effective single-particle potential for the radial wave function of $l=3$ electrons contains two wells separated by a barrier, and the wave function of the $4f$ electron, which is the lowest f electron, collapses into the inner well at $Z=56$ and higher Z. When the collapse occurs, the wave functions of the $4d$ and $4f$ electrons overlap appreciably.

The $4d^{10}4f^7 \rightarrow 4d^9 4f^8$ (denoted $4d \rightarrow 4f$) resonance structure in the absorption spectrum of atomic Eu was first reported by Mansfield and Connerade in 1976,[4] and it closely resembles that of Eu metal.[1] The main feature is the large peak at photon energies near 141 eV. In addition to the large peak, there are small peaks at lower energies. Photoelectron spectra of atomic Eu were measured recently by Becker *et al.*,[8] Meyer *et al.*,[10] and Richter *et al.*,[11] and partial cross sections for $4d$, $4f$, $5s$, $5p$, and $6s$ electrons were reported.[8,10,11]

Amus'ya and co-workers[17,18] have calculated the $4f$, $4d$, $5s$, and $5p$ partial photoionization cross sections of Eu in the photon energy range from 95 to 180 eV, covering the $4d \rightarrow 4f$ resonance peak. They used a method of polarized spins[28,29] in which each subshell of the atom is divided into two subshells, one with all spins up and the other with all spins down. Since the Eu atom has a half-filled $4f$ subshell, this method enabled them to treat it as a closed-shell atom within the random-phase approximation with exchange (RPAE).[30] Recently, Zangwill[19] and Zangwill and Doolen[20] have used the relativistic time-dependent local-density approximation (RTDLDA) method to calculate the Eu photoionization cross section, and the partial cross sections for the $4d, 4f, 5p$, and $6s$ electrons are reported in the photon energy range from 105 to 175 eV. A spherical average over the sublevels due to the open $4f$ subshell is explicitly performed in this approximation.[19]

In this paper we present a calculation of the Eu photoionization cross section based on many-body perturbation theory (MBPT).[31] The main purpose of our study is to calculate the partial cross sections for electrons in the $4d$ subshell and all outer subshells. The partial cross sections of the $4d$, $4f$, $5s$, $5p$, and $6s$ electrons are calculated including correlations among the different single-excitation channels. We also calculated the angular distribution asymmetry parameters β of the photoelectrons from the $4d^{10}$, $4f^7$, and $5p^6$ subshells. Preliminary results of this work have been reported elsewhere,[32,33] but the present paper gives a more detailed account of the calculations, includes higher-order correlations, and also presents new results for the β parameters and the branching ratios of partial cross sections.

In order to obtain relatively accurate threshold positions of the $4d$ excitation channels and also to investigate the LS-multiplet structure, we used the LSM_LM_S angular momentum coupling scheme. We calculated spin-orbit parameters to estimate the size of the spin-orbit splitting for the $4d \rightarrow 4f$ resonance transition and for each of the ionization thresholds. The spin-orbit interactions were neglected in calculations of partial cross sections.

The theory of this calculation is discussed in Sec II. In Sec. III, our results are compared with experiments[8,10,11] and other calculations.[17-20] Our conclusions are given in Sec IV.

II. THEORY

In this calculation we use the electric dipole approximation for photon absorption by atoms. We neglect rela-

tivistic effects including spin-orbit interaction, and we include only singly excited final states. Atomic units are used in this paper.

Our Hamiltonian for the neutral atom with N electrons is

$$H = H_0 + H_c \ , \tag{1}$$

where

$$H_0 = \sum_{i=1}^{N} \left[-\tfrac{1}{2}\nabla_i^2 - \frac{Z}{r_i} + V(r_i) \right] , \tag{2}$$

and

$$H_c = \sum_{i<j=1}^{N} \frac{1}{r_{ij}} - \sum_{i=1}^{N} V(r_i) \ , \tag{3}$$

where the single-particle potential $V(r_i)$ accounts for the average interaction of the ith electron with the remaining $N-1$ electrons, and H_c is treated as a perturbation.[31] When the atom interacts with a external electromagnetic radiation field $F\hat{\epsilon}_z \cos(\omega t)$ with $\hat{\epsilon}_z$ a unit vector in the direction of the field, in the dipole approximation the interaction can be treated as a perturbation,

$$V_{\text{ext}} = F \cos(\omega t) \sum_{i=1}^{N} z_i \ . \tag{4}$$

The zeroth-order wave function Φ is an eigenfunction of H_0 and is calculated in the LS-coupling scheme. It is a linear combination of the Slater determinants of single-particle wave functions, and these orbitals are calculated numerically from the single-particle Schrödinger equation

$$\left[-\tfrac{1}{2}\nabla^2 - \frac{Z}{r} + V(r) \right] \phi_i = \varepsilon_i \phi_i \ , \tag{5}$$

where ε_i is the single-particle energy eigenvalue.

The general form of the potential $V(r)$ used for an excited single-particle state is given by[34]

$$V = R + (1-P)\Omega(1-P) \ , \tag{6}$$

where P is the projection operator given by

$$P = \sum_{n_{\text{occ}}} |n\rangle\langle n| \ , \tag{7}$$

where n_{occ} runs over the occupied ground state orbitals. In Eq. (6) R is the Hartree-Fock (HF) potential used to determine the ground-state orbitals, and Ω may be chosen such that the potential of Eq. (6) enhances the convergence of the perturbation expansion.[30,31] Calculating occupied and excited states of a given angular quantum number l in the same Hermitian potential guarantees orthogonality.

The photoionization cross section is related to the imaginary part of the frequency-dependent dipole polarizability by[35]

$$\sigma(\omega) = \frac{4\pi\omega}{c} \mathrm{Im}\alpha(\omega) \ , \tag{8}$$

where c is the speed of light. The quantity $\mathrm{Im}\alpha(\omega)$ can be expressed in terms of dipole matrix elements. The length-form dipole matrix element is

$$Z_L(p \rightarrow k) = \left\langle \Psi_p{}^k \left| \sum_{i=1}^{N} z_i \right| \Psi_0 \right\rangle , \tag{9}$$

where $|\Psi_0\rangle$ and $|\Psi_p{}^k\rangle$ are the exact ground-state wave function and final-state wave function for the $p \rightarrow k$ transition, respectively. The velocity form dipole matrix element is given by

$$Z_V(p \rightarrow k) = \frac{1}{E_0 - E_f} \left\langle \Psi_p{}^k \left| \sum_{i=1}^{N} \frac{d}{dz_i} \right| \Psi_0 \right\rangle , \tag{10}$$

where E_0 and E_f are energy eigenvalues corresponding to $|\Psi_0\rangle$ and $|\Psi_p{}^k\rangle$, respectively. We use $Z(p \rightarrow k)$ to denote the length-form or the velocity-form dipole matrix element when no indication of the distinction is needed.

The polarizability $\alpha(\omega)$ can be calculated by evaluating a perturbation expansion in powers of H_c. Also, starting from the perturbation expansion for $\alpha(\omega)$, a perturbation expansion for $Z(p \rightarrow k)$ can be derived such that the contribution from the $p \rightarrow k$ ionization channel to $\mathrm{Im}\alpha(\omega)$ is[31]

$$\mathrm{Im}\alpha(\omega) = \frac{2N}{k} |Z(p \rightarrow k)|^2 \ , \tag{11}$$

where N is a normalization correction usually close to unity. The wave number k of the photoelectron is given by $k = \sqrt{2(\omega - I)}$, where I is the ionization energy associated with the p^{-1} residual ion in which the orbital p is missing from the atom. Equation (11) depends on the fact that the radial part of the continuum wave function $P(r) = rR(r)$ is normalized to a sinusoidal function as $r \rightarrow \infty$.[31]

In this case, the partial cross section for the $p \rightarrow k$ ionization channel is

$$\sigma(\omega) = \frac{8\pi\omega N}{ck} |Z(p \rightarrow k)|^2 \ , \tag{12}$$

The perturbation expansion of $Z(p \rightarrow k)$ is represented by a series of open diagrams which have one dipole interaction and any number of interactions with the correlation term H_c given by Eq. (3). Typical diagrams are shown in Fig. 1. In these diagrams, dashed lines with a free end represent the dipole interactions, and dashed lines with no free ends represent the correlation interactions with H_c. Each line with an arrow drawn upward denotes an occupied excited single-particle state (a particle), and each line with an arrow drawn downward denotes a vacancy in the initial state (a hole). The pair of open lines labeled by p and k on top of each diagram represents the final state $|\Phi_p{}^k\rangle$. The "order" of a given diagram refers to the numbers of H_c interactions. Correlation interactions H_c below and above the dipole interaction correspond to correlations in the ground state and the final state, respectively.

The lowest-order diagram of Fig. 1(a) gives the HF results for $Z(p \rightarrow k)$ provided a HF potential is used to calculate the basis states. The exchange diagrams are not explicitly shown in Fig. 1 but are also included. The first-order diagram of Fig. 1(b) contains an H_c interaction in the final state. The coupled-equations method[36] can be used to include the H_c interaction between singly excited

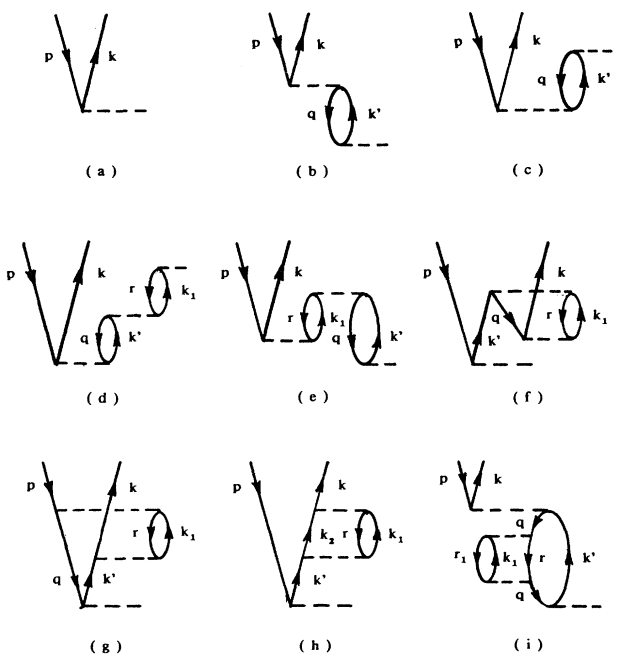

FIG. 1. Diagrams contribution to the matrix element $Z(p \rightarrow k)$. Exchange diagrams (not shown) are also included.

final states to all orders in perturbation theory. It includes those diagrams with any number of H_c interactions above the dipole interaction but having only one particle line and one hole line just above each interaction. This method is essentially a K-matrix method,[37] and it represents the Tamm-Dancoff approximation including exchange contribution.[38]

When interactions between a bound excitation of an inner-subshell electron and the continuum excitations of the outer-subshell electrons are thus treated, a resonance peak appears in the resulting partial cross section of an outer subshell if its ionization threshold is below the excitation energy of the inner-subshell transition. The width of this peak represents the contribution from simple autoionizing processes in which the inner-subshell hole is refilled by the excited electron (or an outer-subshell electron) and an outer-subshell electron (or the excited electron) is ejected into the continuum. There is also a small shift in the position of the resonance peak due to these interactions.

The ground-state correlation diagrams of Figs. 1(c) and 1(d) can be added into the coupled equations. In addition, we can also include in the coupled equations the diagrams of Figs. 1(e) through 1(h), and contributions from higher-order diagrams containing repeated insertions of the diagram segments in Figs. 1(e) through 1(h) above the dipole interaction can be included to a good approximation. Figures 1(e) and 1(f) are second-order final-state correlation diagrams. Figure 1(e) and corresponding higher-order diagrams are included in the RPAE method.[30] Figure 1(g) describes relaxation effects when $p=q$, and Fig. 1(h) describes polarization effects.

If the energy of a bound excitation of an inner-shell electron is high enough, it may also decay through the refilling of the inner-shell hole by an outer-shell electron and the ejection of another outer-shell electron. Processes of this type can be considered as the Auger decay of the ionic core with the excited electron being a spectator if it is in a Rydberg state. These processes also contribute to the width of the corresponding resonance peak in the partial cross section for the outer-shell electrons. Figure 1(i) represents such a situation when $q \rightarrow k'$ is the inner-shell excitation, $p \rightarrow k$ is an outer-subshell ionization channel, k_1 is a continuum state, and r and r_1 are outer shell electrons. By summing over a geometric series including the diagrams of Figs. 1(b) and 1(i), and those with the segment on the q hole line in Fig. 1(i) repeatedly inserted to all orders, we obtain a complex term added to the energy denominator $\varepsilon_q - \varepsilon_{k'} + \omega$. Its real part is an energy shift, and its imaginary part is the contribution to the half-width of the $q \rightarrow k'$ resonance peak from the decay process in which the state $|\Phi_q{}^{k'}\rangle$ decays into the state $|\Phi_{rr_1}{}^{k'k_1}\rangle$.

In the calculation of the angular distribution asymmetry parameter β, the formula we used for a specific residual ionic multiplet i is

$$\beta = \frac{(l+2)(l+1)|Z_{l+1}|^2 + l(l-1)|Z_{l-1}|^2 - 6(l+1)l\,\mathrm{Re}(Z_{l+1}Z_{l-1}{}^* e^{i(\sigma_+ + \delta_+ - \sigma_- - \delta_-)})}{(2l+1)[(l+1)|Z_{l+1}|^2 + l|Z_{l-1}|^2]}, \tag{13}$$

where Z_{l+1} denotes $Z(p \rightarrow k)$ in which the angular quantum numbers of p and k are l and $l+1$, respectively, and Z_{l-1} denotes $Z(p \rightarrow k)$ in which the angular quantum number of k is $l-1$. Coulomb phase shifts σ_+ and σ_- correspond to photoelectrons with orbital angular quantum number $l+1$ and $l-1$, respectively. The corresponding non-Coulomb phase shifts are given by δ_+ and δ_-.

Equation (13) was first derived by Cooper and Zare[39] using the central field approximation in which the radial wave functions and the phase shifts of the photoelectron corresponding to the different multiplets due to the angular momentum coupling between the residual ion and the photoelectron are assumed to be the same. However, following more general treatments[40] of the β parameter, Eq. (13) can be derived as a special case in which the total orbital angular momentum of the atom in the initial state is zero regardless of its total spin. This means that for the photoionization of the ground-state Eu atom, the radial dipole matrix elements and phase shifts calculated using the LS term-dependent effective potential can be used in Eq. (13) to include the effects due to the multiplet struc-

ture of the final state. The values of the radial dipole matrix elements Z_{l+1} and Z_{l-1} are in general complex if the final-state interchannel interactions are included in the calculation.[41]

When several possible residual ionic multiplets are considered at the same time, the β parameter is given by

$$\beta = \frac{\sum_i \sigma_i \beta_i}{\sum_i \sigma_i} , \tag{14}$$

with i running over the ionic multiplets.

III. CALCULATIONS AND RESULTS

The ground state of the Eu atom is $4d^{10}5s^2\ 5p^6 4f^7 6s^2(^8S)$, and all the spins of the $4f$ electrons are aligned. All the final states of dipole transitions have the coupling ^8P, and the $4d^9 4f^8$ resonance state has the coupling $4d^9(^2D)4f^8(^7F)(^8P)$. We included final states with single excitations of one of the $4d$, $5s$, $5p$, $4f$, and $6s$ electrons. When an electron other than $4f$ is excited, we only included those final states in which the coupling of the $4f^7$ subshell is the same as its ground state coupling ^8S. Transitions into the final states in which the coupling of the $4f^7$ subshell is different from ^8S are assumed to be relatively weak because the lowest diagram of Fig. 1(a) is zero for these states, which means that they are accessible only after inclusion of electron correlation effects. The ionization channels that we included are listed in Table I.

The ground-state wave functions of the Eu atom were calculated with the computer program MCHF77, of Froese-Fischer.[42] The spin-orbit parameters computed with this program were used to estimate the spin-orbit effects. The calculated spin-orbit parameters ξ_{4d}, ξ_{4f}, and ξ_{5p} are 2.0, 0.19, and 2.0 eV, respectively. For each of the ionization channels, eight excited bound states and twenty-six continuum states were calculated and used in the coupled equations.[36]

TABLE I. Ionization channels and energies.

Final state[a]	Ionization energy[b] (eV)
$4d^9 4f^7(^7D)kf, kp$	159.8
$4d^9 4f^7(^9D)kf, kp$	139.6
$4f^7 5s(^7S)kp$	49.3
$4f^7 5s(^9S)kp$	45.7
$4f^7 5p^5(^7P)kd, ks$	28.8
$4f^7 5p^5(^9P)kd, ks$	25.7
$4f^6(^7F)kg, kd$	12.9
$4f^7 6s(^7S)kp$	4.6
$4f^7 6s(^9S)kp$	4.4

[a]Here the coupling of the $4f^7$ subshell is always ^8S, and all final states are ^8P.

[b]The listed energy values are calculated by taking differences of self-consistent field (SCF) solutions.

We compared the self-consistent solutions of the $4d$ and $4f$ wave functions in the ground state and the $4d^9 4f^8(^8P)$ resonance state. The overlap integral of the $4d$ orbitals is 0.999 98, and the overlap integral of the $4f$ orbitals is 0.999 99. They indicate that the effects of relaxation on these orbitals are very small for the $4d^9 4f^8(^8P)$ resonance state.

The threshold energy values that we used are the difference in self-consistent field (ΔSCF) values, and they are also listed in Table I. The ΔSCF energy is the difference between the energy of the residual ion and the energy of the ground-state atom given by the self-consistent HF solutions.

Becker *et al.* have reported two $4d$ threshold.[8] One at approximately 137 eV was assigned to the $4d_{5/2}$ electrons, and one at approximately 142 eV was assigned to the $4d_{3/2}$ electrons. The positions of these two levels measured by Richter *et al.*[11] are at 137.6 and 142.5 eV, respectively. Our calculated $4d^{-1}(^9D)$ ionic level is at 139.6 eV, and our first-order perturbation calculation of the spin-orbit splitting by applying the *LSJ* coupling scheme to this ionic state shows five spin-orbit levels ranging from 137.2 to 141.6 eV. The measured and calculated ranges of spin-orbit splitting agree well. However, the five calculated ($^9D_{6,5,4,3,2}$) levels do not form two groups which can be identified with the two measured levels. This indicates that the mixing among the corresponding J-sublevels of the different multiplets of the $4d^9 4f^7$ configuration should be investigated in further studies of the spin-orbit splitting of the $4d$ threshold.

Our calculated $4d^{-1}(^7D)$ ionic level is at 159.8 eV, and the separation between the $4d^{-1}(^7D)$ and the $4d^{-1}(^9D)$ levels is 20.1 eV. This separation is mainly due to the large exchange interaction between the $4d$ and $4f$ electrons, and it is much larger than our calculated 4.4 eV range for the spin-orbit splitting in the $4d^{-1}(^9D)$ level. It is also much larger than the 5.49 eV separation between the $4d_{3/2}$ and the $4d_{5/2}$ single-particle energies given by a relativistic calculation[43] in which the Dirac-Fock equations for the Eu atom were solved. For this reason, we used the *LS* coupling scheme in our calculation as a first approximation.

The ΔSCF value for the excitation energy of the $4d^9 4f^8(^8P)$ resonance state is 146.9 eV. It is calculated by taking the difference between the self-consistent HF solutions for the resonance state and the ground state. We also calculated the second-order energy corrections which are not included in the ΔSCF value, and the calculated $4d \rightarrow 4f$ excitation energy including these corrections is 145.5 eV. The energy shift given by the coupled equations is approximately -4.5 eV, and this shift is mainly due to the interactions which cause the autoionizing decay of the resonance. That is, this shift is due to correlations in the $4d^9 4f^8$ level in which one $4f$ electron makes a virtual transition to the empty $4d$ state and another $4f$ electron is excited to an unoccupied bound level or to the continuum. The $4d \rightarrow 4f$ resonance peak appears at approximately 141 eV in our calculated total cross section, which agrees with experimental results.[4,8,10,11]

We calculated diagrams (a), (b), and (c) of Fig. 1 for all

of the $p \rightarrow k$ channels listed in Table I using the coupled equations method, and so higher-order diagrams similar to Fig. 1(b) were included to all orders.

Second-order ground-state correlation diagrams such as Fig. 1(d) were calculated for the cases where $p \rightarrow k$ is $4f \rightarrow kg$, $5p \rightarrow ({}^9D, {}^7D)kd$, or $4d \rightarrow 4f$. These diagrams improved the agreement between the length form and the velocity form cross sections near the $4d \rightarrow 4f$ resonance.

We also included some second-order final-state correlation diagrams in solving the coupled equations. The diagrams of Figs. 1(e) and 1(f) and the other time ordering of these diagrams were calculated for cases where q is $4d$, k' is $4f$, and $p \rightarrow k$ is $4f \rightarrow kg$, $4d \rightarrow ({}^9D)kf$, $5p \rightarrow ({}^9P, {}^7P)kd$, or $5s \rightarrow ({}^9S, {}^7S)kp$. Figure 1(g), the other time ordering of Fig. 1(g), and Fig. 1(h) were evaluated when $p \rightarrow k$ is $4d \rightarrow ({}^9D)kf$ and $q \rightarrow k'$ and $p \rightarrow k'$ are $4d \rightarrow 4f$.

The contributions of Auger decays to the resonance widths, as described in Fig. 1(i), were calculated for the $4d \rightarrow 4f$, $4d \rightarrow ({}^9D)nf, np$, and $4d \rightarrow ({}^7D)nf, np$ resonances.

In Fig. 2 our results for the total cross section in the photon energy range 100–210 eV are compared with the experimental results. The results of the photoelectron yield given by Becker *et al.*[8] and the total absorption results of Mansfield and Connerade[4] are in arbitrary units. We normalized the results of Becker *et al.* to ours at the photon energy 123 eV, and we normalized the results of Mansfield and Connerade to those of Becker *et al.* at the peak of the $4d \rightarrow 4f$ resonance. Richter *et al.*[11] normalized their partial $4f$ cross section to the calculated cross section by Zangwill and Doolen[20] and our earlier MBPT calculation[32] in the energy range above the $4d \rightarrow 4f$ resonance. The overall agreement between results of our calculation and the experiments is good, and the agreement between the calculated length-form and velocity-form results is reasonable. If we sum over the $4d$, $4f$, and $5p$ partial cross sections calculated by Zangwill and Doolen,[19] the results will also be quite close to our total cross section. The width of the $4d \rightarrow 4f$ resonance peak in Fig. 2 is approximately 7 eV, and it is dominated by contributions of autoionizing decay leading to continua of the $4d$, $4f$, $5s$, $5p$, and $6s$ excitations.

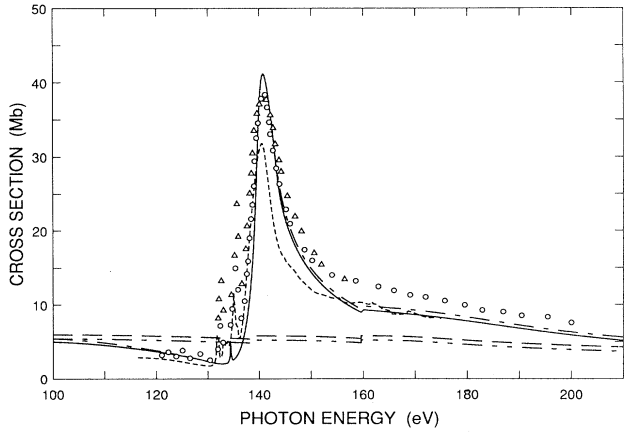

FIG. 2. Total cross section near the $4d^{10}4f^7 \rightarrow 4d^9 4f^8$ resonance. Circles, results of total electron yield measured by Becker *et al.* (Ref. 8); triangles, results of total absorption measurement by Mansfield and Connerade (Ref. 4); -----, total absorption results of Richter *et al.* (Ref. 11). We normalize the relative results of Becker *et al.* to ours at 123 eV. We normalized the relative results of Mansfield and Connerade to those of Becker *et al.* at the peak of the $4d \rightarrow 4f$ resonance. Richter *et al.* normalized their $4f$ partial cross section to the calculated RTDLDA results of Ref. 20 and the MBPT results of Ref. 32 above the $4d \rightarrow 4f$ resonance. Other curves are sums of partial cross sections calcualted in this work: ——, length-form calculated total cross section; —·—·— velocity-form calculated total cross section; — — — length-form HF results; ··––, velocity-form HF results.

The differences between the results of Becker *et al.*[8] and those of Richter *et al.*[11] are mainly due to the fact that they are normalized differently in the figure. If we normalize the results of Becker *et al.* to those of Richter *et al.* at the photon energy of 170 eV, then the two sets of results will agree very well except at the $4d \rightarrow 4f$ resonance and will be only slightly different at the resonance peak. We have normalized the results of Becker *et al.*[8] to our calculated results at a photon energy below the $4d \rightarrow 4f$ resonance because we did not include those $4d^{-1}kf, kp$ final states in which the coupling of the $4f^7$ subshell is not ${}^8S$ and did not include final states of $4d$ photoionization with simultaneous excitation of an outer subshell electron. Many of these final-state channels become open in the 30 eV energy range above the $4d \rightarrow 4f$ resonance, and their contributions to the total cross section may not be negligible. Indeed, our results are 20–30 % lower than those of Becker *et al.*[8] above the $4d \rightarrow 4f$ resonance, which is possibly due to this reason.

The calculated results are higher than experimental results at the $4d \rightarrow 4f$ resonance peak. A possible reason is that we neglected spin-orbit interactions in calculating the cross section. The shifts of the $4d^9 4f^8({}^8P)$ resonance state from the LS-coupling value due to spin-orbit interactions obtained in a first-order perturbation calculation using the LSJ-coupling scheme are -0.80, 0.23, and 1.03 eV for the ${}^8P_{9/2}$, ${}^8P_{7/2}$, and ${}^8P_{5/2}$ states, respectively. The resonance peak we obtained without spin-orbit effects of the resonance states is expected to be somewhat higher and narrower than the one when the spin-orbit splitting of the resonance state is included.

Moreover, the five calculated $4d^{-1}({}^9D_{6,5,4,3,2})$ ionic levels range from 137.2 to 141.6 eV, some above the $4d \rightarrow 4f$ resonance and some below it. The ionization channels associated with those levels above the resonance have no peak structure in their partial cross sections and also do not contribute to the linewidth of the resonance peak. Thus, including the spin-orbit splitting of the $4d^{-1}({}^9D)$ ionic level may reduce both the height and width of the $4d \rightarrow 4f$ resonance peak in the total cross section.

The small structures prior to the large peak in the experimental results were attributed to spin-orbit effects involving other multiplets than ${}^8P$ of the $4d^9 4f^8$ configuration,[2] and they were not calculated since we neglected spin-orbit interactions. The small peak at 134.5 eV in the calculated results is the $4d \rightarrow ({}^9D)6p$ reso-

nance, and other $4d \rightarrow (^9D)np, nf$ resonances are very weak. No individual resonance peak of the $4d \rightarrow (^7D)np, nf$ series can be seen in the calculated total cross section. The widths of the $4d \rightarrow (^9D, ^7D)np, nf$ resonance peaks are dominated by contributions of the Auger decay transitions of the $4d^{-1}(^9D, ^7D)$ ionic states. The Auger linewidths obtained by evaluating the lowest-order contributions are 0.15 and 1.6 eV for the ^9D and the ^7D states, respectively. The width for the ^7D state is much larger since, due to the different symmetries of the $4d^{-1}(^9D, ^7D)$ ionic states, a $4f$ electron cannot fill the $4d$ hole in the ^9D state in an Auger transition but can fill the $4d$ hole in the ^7D state. Thus the transition in the Auger decay of the ^7D ionic state can be a super Coster-Kronig transition in which the hole state and the two outer-subshell electorns have the same principal quantum number,[44] and it leads to a large Auger line width.

Our calculated partial cross sections of the $4f$, $4d$, $5p$, $5s$, and $6s$ electrons are shown in Figs. 3, 4, and 5 and compared with experimental results[8,10,11] and other calculated results.[17–20] The geometric mean of our length-form and velocity-form results is presented, and the discrepancy between our length-form and velocity-form cross sections is similar to that of our total cross-section curves shown in Fig. 2. The experimental results of Becker *et al.*[8] and Meyer *et al.*[10] are in arbitrary units, and we normalized the $4f$ cross section of Becker *et al.* to ours at 111 eV. We renormalized the $4f$ cross section of Meyer *et al.* to that of Becker *et al.* at the peak of the $4d \rightarrow 4f$ resonance. The other partial cross sections of Becker *et al.* and Meyer *et al.* were measured relative to their $4f$ cross sections, respectively. The results measured by Richter *et al.*[11] were normalized to theoretical cross sections[20,32] in the energy range above the resonance.

The overall agreement between our results and the experimental results is reasonably good. These results show that the autoionizing decay of the $4d \rightarrow 4f$ resonance in the Eu atom is mainly through $4f$ ionization channels, in agreement with the calculation of Amus'ya *et al.*[17] The possibilities of decay through ionization channels of other electrons are in descending order of $4d$, $5p$, $5s$, and $6s$. At approximately 135 eV there is a minimum in the 4f partial cross section prior to the $4d \rightarrow 4f$ resonance, but no similar minimum can be found in the $5s$, $5p$, and $6s$ partial cross sections. Our calculated partial cross sections presented here and reported previously[32] are lower than our preliminary results[33] by about 20% at the $4d \rightarrow 4f$ resonance peak. We attribute this to higher-order many-body effects included in the present calculations by use of the coupled-equations method.

In Fig. 3 we also present results by Amus'ya, Sheftel, and Chernysheva[17] and by Amusia, Ivanov, and Kupchenko.[18] Both calculations used the spin-polarized random-phase approximation method.[15] In our calculation the $4d \rightarrow (^9D)kp, kf$ channels also contribute to the decay pathways of the $4d \rightarrow 4f$ resonance since the $4d^{-1}(^9D)$ ionic level is below the $4d^9 4f^8(^8P)$ level. We found in our calculation that the contributions of the $4d \rightarrow (^9D)kp, kf$ channels to the width of the $4d \rightarrow 4f$ resonance peak were sensitive to the energy difference between the two levels. In self-consistent solutions, energy positions of the $4d_\downarrow^{-1}$ and $4d_\uparrow^{-1}$ ionic levels in the polarized-spins model[17,18] of the Eu atom may be different from the positions of the $4d^{-1}(^9D)$ and $4d^{-1}(^7D)$ levels in the LS-coupling scheme. Here the notations $4d_\downarrow$ and $4d_\uparrow$ refer to $4d$ electrons with spins down and up, respectively. Thus the widths and heights of the $4d \rightarrow 4f$ resonance peaks may be different in the two calculations using the two different angular momentum coupling schemes. The energy positions of the $4d_\downarrow^{-1}$ and $4d_\uparrow^{-1}$ ionic levels in the calculations of Amus'ya *et al.*[17,18] were not reported and so cannot be compared here with the $4d^{-1}(^9D, ^7D)$ ionic levels in our calculation. However, the calculated separation[17] between the $4d_\downarrow^{-1}$ and the $4d_\uparrow^{-1}$ ionic levels is 16.94 eV, and our result of separation between the $4d^{-1}(^9D)$ and $4d^{-1}(^7D)$ levels is 20.1 eV. In the RTDLDA calculation of Zangwill,[19] the different $4d^{-1}$ sublevels were averaged over to give a single $4d$ threshold at approximately 133 eV. Because of this, the contribution of the $4d$ ionization channel to the width of the $4d \rightarrow 4f$ resonance is different from those in the other two calculations, and so are the width and height of the $4d \rightarrow 4f$ resonance peak in the cross section.

Richter *et al.*[11] adapted an absolute scale for their measured cross sections by normalizing their $4f$ partial cross section to the results of the RTDLDA calculation by Zangwill and Doolen[20] and our previous MBPT calculation,[32] above the $4d \rightarrow 4f$ resonance. In Fig. 3, the $4f$ cross sections measured by Becker *et al.*[8] and Meyer

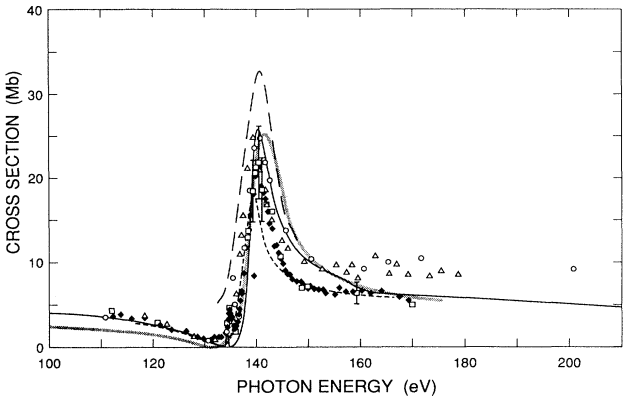

FIG. 3. Partial $4f$ cross section near the $4d \rightarrow 4f$ resonance. Circles, experimental results of Becker *et al.* (Ref. 8); triangles, experimental results of Meyer *et al.* (Ref. 10); squares and diamonds, experimental results of Richter *et al.* (Ref. 11). We normalized the relative results of Becker *et al.* to our calculated results at 111 eV. We normalized the results of Meyer *et al.* to those of Becker *et al.* at the peak of the $4d \rightarrow 4f$ resonance. The results of Richter *et al.* were normalized to the calculations of Refs. 20 and 32. Curves are theoretical results: ——, this calculation; — — —, $4f \rightarrow kg$ cross section of Amus'ya *et al* (Ref. 17); -----, RTDLDA calculation by Zangwill (Ref. 19). The thick grey line is the spin-polarized RPAE calculation by Amusia *et al.* (Ref. 18).

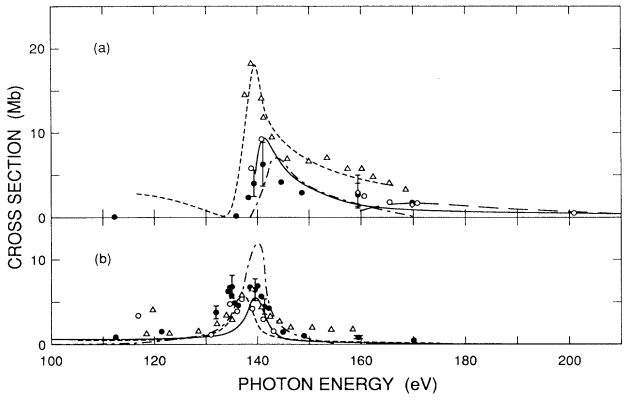

FIG. 4. Partial cross sections of the $4d$ and $5p$ electrons near the $4d \rightarrow 4f$ resonance. Circles, experimental results of Becker *et al*, (Ref. 8); triangles experimental results of Meyer *et al.* (Ref. 10); solid circles and diamonds, experimental results of Richter *et al.* (Ref. 11). These results were measured relative to the corresponding $4f$ experimental cross section. -----, results of the RTDLDA calculations (Refs. 19 and 20); —— and — — —, this calculation; —·—·— spin-polarized RPAE calculation by Amusia *et al.* (Ref. 18). (a) σ_{4d} cross section. The solid curve and long-dashed curve are our calculated $\sigma_{4d\rightarrow(^9D)k}$ and $\sigma_{4d\rightarrow(^7D)k}$ cross sections, respectively. (b) σ_{5p} cross section.

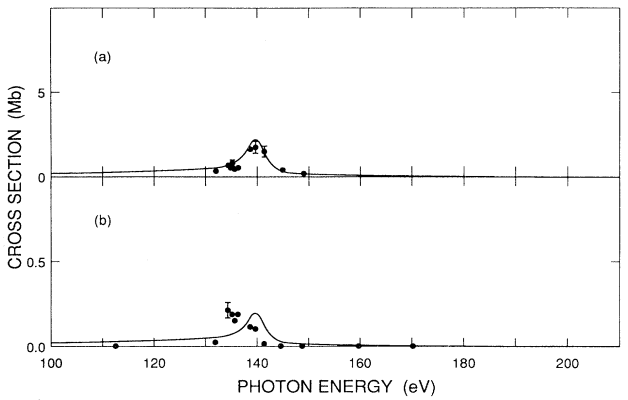

FIG. 5. Partial cross sections of the $5s$ and $6s$ electrons near the $4d \rightarrow 4f$ resonance. Solid circles, experimental results of Richter *et al.* (Ref. 11). ——, this calculation. (a) σ_{5s}, (b) σ_{6s}.

et al.[10] appear to be higher than that of Richter *et al.*[11] by about 30% above the $4d \rightarrow 4f$ resonance. However, one can normalize the results of Becker *et al.* and Meyer *et al.* so that they are higher than the results of Richter *et al.* by about 15% above the resonance and lower by about 15% below the resonance. Thus the three sets of measured results agree within the experimental error bars. If the $4d^{-1}(^7D)k$ component which we predict above 160 eV does appear, then the $4d$ and $4f$ partial cross sections of Becker *et al.*[8] have to be reduced by approximately 20% because their results are normalized to the total electron yield.[45] In that case the agreement between their experiment and our calculation will be better.

The results for $4d$ and $5p$ partial cross sections are compared in Figs. 4(a) and 4(b), respectively. The $4d$ cross section of the RTDLDA calculation by Zangwill is given by the short-dashed curve in Fig. 4(a) and is substantially higher than our $4d^{-1}(^9D)k$ cross section. With a single $4d$ threshold located at a relatively low energy, the interaction between the $4d$ ionization channel and the $4d \rightarrow 4f$ transition in the RTDLDA calculation is stronger than in our calculation. The RTDLDA results agree well with the measured results of Meyer *et al.*,[10] but the results of Meyer *et al.* are also substantially higher than the measured results of Becker *et al.*[8] and Richter *et al.*[11] In Fig 4(a) the curve with the long and short dashes is the $4d_{\downarrow}$ cross section calculated by Amusia *et al.*[18] The $4d$ cross-section data near the threshold were obtained by measuring the Auger electrons.[8,10,11] In the measured photon energy range there are many possible channels of ionization with excitation and double excitation, and their corresponding Auger lines may be close to each other. The discrepancy between the results of Meyer *et al.* and the results of Becker *et al.* and Richter *et al.* may be caused by the fact that the Auger lines were resolved differently in these experiments.

Our $4d \rightarrow (^9D)k$ cross section begins at 139.6 eV, just below the $4d \rightarrow 4f$ resonance at 141 eV. Since we did not include spin-orbit interactions, the $4d$ cross section we calculated may be a rough approximation near the $4d \rightarrow 4f$ resonance, although it appears to agree fairly well with the measured results of Becker *et al.*[8] and Richter *et al.*[11] at the main resonance peak. Our $4d \rightarrow (^7D)k$ cross section begins at 159.8 eV. There are four other $4d^9 4f^7(^7D)$ ionic states in which the coupling of the $4f^7$ subshell is ^6P, ^6D, ^6F, and ^6G, respectively. The ΔSCF values for the energy positions of these states range from 150 to 154 eV. Because of the interactions among these states and the $4d^9 4f^7(^8S)(^7D)$ state, the five resulting $4d^9 4f^7(^7D)$ levels may spread out in a wider energy range. This is a possible reason why there has been no observed ionic line at photon energies near 159.8 eV.

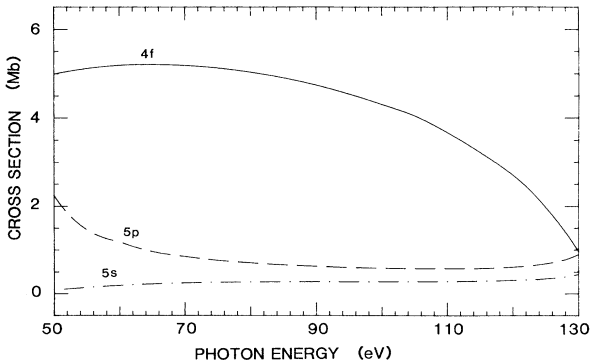

FIG. 6. Partial cross sections of the $4f$, $5s$, and $5p$ electrons between 50 and 130 eV. Geometric means of length form and velocity form results of this work are shown. ——, σ_{4f}; — — —, σ_{5p}; —·—·—·, σ_{5s}.

In our $5p$ partial cross section, the main $4d \rightarrow 4f$ resonance peak has a height close to those in the measured results of Becker *et al.*,[8] Meyer *et al.*,[10] Richter *et al.*,[11] and the results of the RTDLDA calculation.[20]

In Figs. 5(a) and 5(b) our $5s$ and $6s$ partial cross sections are compared with the experimental results of Richter *et al.*[11] The height of the calculated $4d \rightarrow 4f$ resonance peak is close to that of the measured results in both cases.

It can be seen from the experimental results that the structures below the main $4d \rightarrow 4f$ resonance peak are relatively strong in the $5s$, $5p$, and $6s$ partial cross sections. These structures are not treated in all three theoretical calculations compared here.

Our calculated $4f$, $5s$, and $5p$ partial cross sections in the photon energy range from 50 eV up to the vicinity of the $4d \rightarrow 4f$ resonance are compared in Fig. 6. Our calculated $4d$, $4f$, $5s$, and $5p$ partial cross sections in the photon energy range from 170 to 730 eV are compared in Fig. 7. The $6s$ partial cross section is relatively quite small at these photon energies and is not plotted here. From Figs. 3 through 7 it is clear that the $4f$ cross section dominates the total cross section for photon energies between 50 and 300 eV except for a small range of about 10 eV centered at the minimum just below the $4d \rightarrow 4f$ resonance. There is a minimum in the $4d$ cross section at approximately 240 eV because the Cooper minima in the $4d \rightarrow ({}^9D)kf$ and $4d \rightarrow ({}^7D)kf$ partial cross sections are in this region. The $4d$ cross section increases above the minimum and reaches a maximum at a photon energy between 400 and 500 eV. Above the $4d \rightarrow 4f$ resonance, the $4f$ cross section decreases as the photon energy increases but remains larger than the $4d$ cross section until the photon energy reaches approximately 440 eV.

In Fig. 8(a) the $5s \rightarrow ({}^9S)kp$ and $5s \rightarrow ({}^7S)kp$ partial cross sections near the $4d \rightarrow 4f$ resonance are plotted for comparison. Interactions of the $4d \rightarrow 4f$ resonance with these two ionization channels are of different strengths. The branching ratio between the two channels, $\sigma_{5s \rightarrow ({}^9S)kp} / \sigma_{5s \rightarrow ({}^7P)k} p$, is shown in Fig 8(b) along with

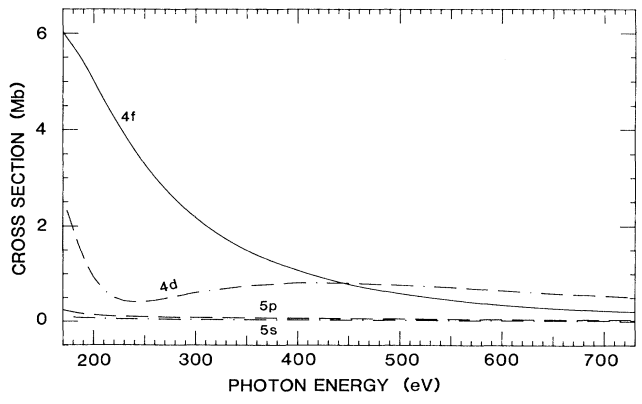

FIG. 7. Partial cross sections for the $4d$, $4f$, $5s$, and $5p$ electrons between 170 and 730 eV. Geometric mean of length form and velocity form results from this work is shown. ——, σ_{4f}; ·---, σ_{4d}; — — —, σ_{5p}; —·—·—·, σ_{5s}.

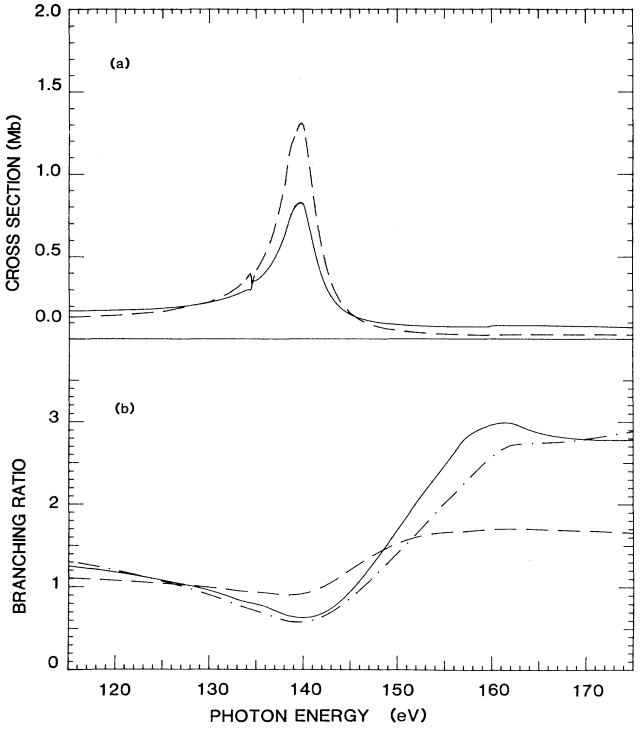

FIG. 8. Partial cross sections corresponding to $5s^{-1}({}^9D)$ and $5s^{-1}({}^7D)$ and the related branching ratios. (a) ——, $\sigma_{5s \rightarrow ({}^9S)kp}$; — — —, $\sigma_{5s \rightarrow ({}^7S)kp}$. The geometric means of the length-form and velocity-form results are shown. (b) ——, $\sigma_{5s \rightarrow ({}^9S)kp} / \sigma_{5s \rightarrow ({}^7S)kp}$; — — —, $\sigma_{6s \rightarrow ({}^9S)kp} / \sigma_{6s \rightarrow ({}^7S)kp}$; —·—·—·, $\sigma_{5p \rightarrow ({}^9P)k} / \sigma_{5p \rightarrow ({}^7P)k}$. These branching ratios are calculated from the geometric mean of the length and velocity form cross sections. The detailed structures due to the $4d \rightarrow ({}^9D, {}^7D)np, nf$ resonances are not mapped out.

branching ratios $\sigma_{6s \rightarrow ({}^9S)kp} / \sigma_{6s \rightarrow ({}^7S)kp}$ and $\sigma_{5p \rightarrow ({}^9P)k} / \sigma_{5p \rightarrow ({}^7P)k}$. The detailed structures due to $4d \rightarrow ({}^9D, {}^7D)np, nf$ resonances are not mapped out. These branching ratio curves all show similar behavior close to the $4d \rightarrow 4f$ resonance. The Eu atom in the ground state has a half-filled $4f$ subshell with all the spins aligned. If we assume all the spins of the $4f$ electrons in the ground state are upward, then the spin of the electron k is downward in a $({}^9L)k$ final state but upward in a $({}^7L)k$ final state. In the $4d^9 4f^8$ resonance state, a $4d$ electron with a downward spin is excited from the initial state to the $4f$ subshell without changing the orientation of its spin. Due to the cancellation between direct and exchange terms, the matrix element $\langle \Phi(p^{-1}k) | H_c | \Phi(4d^9 4f^8) \rangle$ for a $({}^9L)k$ final state is smaller than the matrix element for the corresponding $({}^7L)k$ final state. Thus a $({}^9L)k$ cross section is lower than the corresponding $({}^7L)k$ cross section at the $4d \rightarrow 4f$ resonance peak, although it is higher away from the resonance.

Our results for the angular asymmetry β parameters for the ejection of $4f$, $5p$, and $4d$ electrons are presented

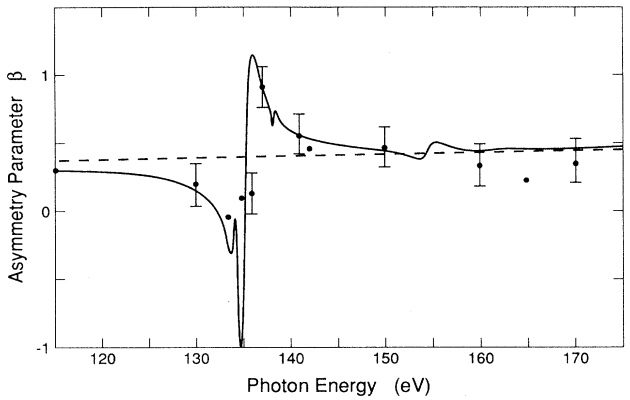

FIG. 9. Asymmetry parameter β_{4f} near the $4d \rightarrow 4f$ resonance. Solid circles, experimental results of Becker and coworkers (Ref. 46). Only the calculated length-form results are plotted here because the differences between the length-form and the velocity-form results are small. ——, results calculated including correlation effects; — — —, results of the HF approximation.

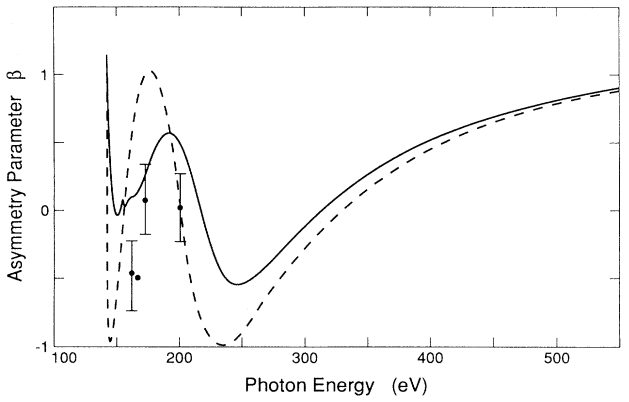

FIG. 11. Asymmetry parameter $\beta_{4d^{-1}(^9D)}$. Curves and symbols are defined as for Fig. 9.

in Figs. 9 through 12 and compared with the experimental results of Becker, Kerkhoff, and co-workers.[46] The differences between the calculated length-form and velocity-form results are small, and we plot here only the length-form results.

In Fig. 9 the results for β_{4f} in the photon energy range 115–175 eV are shown. In the HF approximation, β_{4f} varies slowly as a function of photon energy. After the final-state interchannel interactions are included, the results show an abrupt change in the vicinity of 135 eV, where the $4f$ partial cross section reaches a minimum. The reason for this is that the dipole matrix element for the $4f \rightarrow kg$ channel changes by a phase factor of approximately -1 at this photon energy due to the interaction with the $4d \rightarrow 4f$ resonant transition. Our results including effects of electron correlations agree reasonably with the experimental results, given that the spin-orbit effects, which split the $4d^9 4f^8(^8P)$ resonance state and mix different LS multiplets in this state, are not treated.

Shown in Fig. 10 are our results of β_{5p} obtained from the β parameters corresponding to the $5p^{-1}(^9P)$ and $5p^{-1}(^7P)$ residual ions according to Eq. (14). The results show significant changes over a photon energy range greater than 100 eV after including the interchannel interaction. The structure which peaks at 137 eV, in the measured results in the photon energy range 134–140 eV, is not seen in the calculated results, and one possible reason is that the mixing of different LS multiplets in the $4d^9 4f^8$ resonance state due to the spin-orbit interaction is not treated in our calculation. Otherwise, our results including effects of electron correlations agree fairly well with the measured results.

The β parameters corresponding to the $4d^{-1}(^9D)$ and $4d^{-1}(^7D)$ residual ions are shown in Figs. 11 and 12, respectively. In both cases the results including correlation effects differ appreciably from the HF results over a wide photon energy range above the threshold. In Fig. 11 the agreement between the calculated and the measured re-

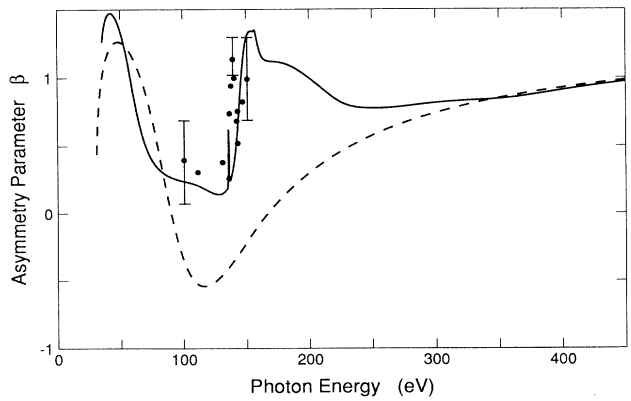

FIG. 10. Asymmetry parameter β_{5p}. We have averaged $\beta_{5p^{-1}(^9P)}$ and $\beta_{5p^{-1}(^7P)}$ using Eq. (14). Curves and symbols are defined as in Fig. 9.

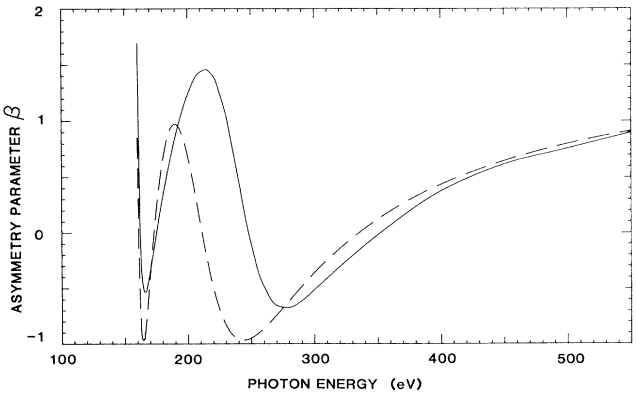

FIG. 12. Asymmetry parameter $\beta_{4d^{-1}(^7D)}$. Calculated curves are defined as for Fig. 9.

sults is not satisfactory, indicating the need in future theoretical studies to investigate the effects of interactions between the $4d^9 4f^7(^9D, ^7D)kf, kp$ channels and other possible $4d^9 4f^7 kf, kp$ channels that are not treated in the present work.

The small structures in β_{4f} and β_{5p} at 134 eV are due to the $4d \rightarrow (^9D)6p$ transition, and the small structure in β_{4f} at 138 eV is due to the $4d \rightarrow (^9D)5f$ transition. The small structures in β_{4f}, β_{5p}, and $\beta_{4d^{-1}}(^9D)$ at 154 eV are due to the $4d \rightarrow (^7D)6p$ transition followed by other transitions in the $4d \rightarrow (^7D)np, nf$ series. Accurate theoretical predictions for the energy positions of the Rydberg states due to excitation of the $4d$ electrons apparently require calculations of higher-order corrections to the energies including spin-orbit effects, and such calculations are beyond the goal of the present study.

IV. CONCLUDING REMARKS

We have calculated the photoionization cross section and the asymmetry parameters β of the Eu atom including effects of electron correlations using many-body perturbation theory (MBPT). Our study focused on the photon energy range near the $4d^{10}4f^7 \rightarrow 4d^9 4f^8$ resonance and included effects of the final-state interchannel interactions; and partial cross sections were calculated for photon energies from 50 to 730 eV. Our calculations agree reasonably well with experiments even though spin-orbit effects were not included. Our results also agree reasonably with those of the previous calculations by Amus'ya *et al.*[17,18] in the energy range 95–180 eV and the recent calculations by Zangwill[19] and Zangwill and Doolen[20] in the energy range 105–175 eV. Comparisons with experimental data beyond the presently measured photon energy range would be interesting.

ACKNOWLEDGMENTS

This work was supported by the United States National Science Foundation. We thank the Academic Computing Center of the University of Virginia for a generous computing grant. We are grateful to Dr. U. Becker, Dr. H. Kerkhoff, and Professor B. Sonntag for helpful discussions of the experimental results. We also thank Dr. L. J. Garvin and Dr. S. Salomonson for helpful discussions.

[1]T. M. Zimkina, V. A. Fomichev, S. A. Gribovskii, and I. I. Zhukova, Fiz. Tverd. Tela. **9**, 1447 (1976) [Sov. Phys. Solid State **9**, 1128 (1967)]; V. A. Fomichev, T. M. Zimkina, S. A. Gribovskii, and I. I. Zhukova, Fiz. Tverd. Tela. **9**, 1490 (1967) [Sov. Phys. Solid State **9**, 1163 (1967)].

[2]J. L. Dehmer, A. F. Starace, U. Fano, J. Sugar, and J. W. Cooper, Phys Rev. Lett. **26**, 1521 (1971).

[3]R. Haensel, P. Rabe, and B. Sonntag, Solid State Commun. **8**, 1845 (1970).

[4]M. W. D. Mansfield and J. P. Connerade, Proc. R. Soc. London Ser. **A352**, 125 (1976).

[5]H. W. Wolff, R. Bruhn, K. Radler, and B. Sonntag, Phys. Lett. **59A**, 67 (1976).

[6]E. R. Radtke, J. Phys. B **12**, L71 (1979); **12**, L77 (1979).

[7]J. P. Connerade and M. Pantelouris, J. Phys. B **17**, L173 (1984).

[8]U. Becker, H. G. Kerkhoff, D. W. Lindle, P. H. Kobrin, T. A. Ferret, P. A. Heimann, C. M. Truesdale, and D. A. Shirley, Phys. Rev. A **34**, 2858 (1986).

[9]Th. Prescher, M. Richter, E. Schmidt, B. Sonntag, and H. E. Wetzel, J. Phys. B **19**, 1645 (1986).

[10]M. Meyer, Th. Prescher, E. von Raven, M. Richter, E. Schmidt, B. Sonntag, and H. E. Wezel, in *Giant Resonances in Atoms, Molecules, and Solids,* edited by J. P. Connerade, J. M. Esteva, and R. C. Karnatak (Plenum, New York, 1987); Z. Phys. D **2**, 347 (1986).

[11]M. Richter, M. Meyer, M. Pahler, T. Prescher, E. V. Raven, B. Sonntag, and H. -E. Wetzel, Phys. Rev. A **40**, 7007 (1989).

[12]A. F. Starace, Phys. Rev. B **5**, 1773 (1972); J. Sugar, *ibid.* **5**, 1785 (1972).

[13]A. F. Starace, J. Phys. B **7**, 14 (1974); G. Wendin and A. F. Starice, *ibid.* **11**, 4119 (1978).

[14]G. Wendin, in *Photoionization and other Probes of Many-Electron Interactions,* edited by F. J. Wuilleumier (Plenum, New York, 1976).

[15]M. Ya. Amusia, V. K. Dolmatov, and V. K. Ivanov, Zh. Eksp. Teor. Fiz. **85**, 115 (1983) [Sov. Phys.—JETP **58**, 67 (1983)].

[16]A. Zangwill and P. Soven, Phys. Rev. Lett. **45**, 204 (1980).

[17]M. Ya. Amus'ya, S. I. Sheftel, and L. V. Chernysheva, Zh. Tekh. Fiz. **51**, 2441 (1981) [Sov. Phys.—Tech. Phys. **26**, 1444 (1981)].

[18]M. Ya. Amusia, V. K. Ivanov, and V. A. Kupchenko, Z. Phys. D **14**, 219 (1989).

[19]A. Zangwill, J. Phys. C **20**, L627 (1987).

[20]A. Zangwill and G. Doolen (unpublished), as presented in Ref. 11.

[21]M. Geoppert-Mayer, Phys. Rev. **60**, 184 (1941).

[22]J. W. Cooper, Phys. Rev. Lett. **13**, 762 (1964).

[23]D. C. Griffin, K. L. Andrew, and R. D. Cowan, Phys. Rev. **177**, 62 (1969).

[24]J. P. Connerade, Contemp. Phys. **19**, 415 (1978).

[25]I. M. Band, V. I. Fomichev, and M. B. Trzhaskovskaya, J. Phys. B **14**, 1103 (1981).

[26]R. I. Karaziya, Usp. Fiz. Nauk. **135**, 79 (1981) [Sov. Phys.—Usp. **24**, 775 (1981)].

[27]K. T. Cheng and C. Froese Fischer, Phys. Rev. A **28**, 2811 (1983).

[28]H. P. Kelly and A. Ron, Phys. Rev. A **5**, 168 (1972); Phys. Rev. Lett. **26**, 1359 (1971).

[29]M. Ya. Amusia, V. K. Ivanov, and L. V. Chernysheva, J. Phys. B **14**, L19 (1981).

[30]M. Ya. Amusia and N. A. Cherepkov, Case Studies Phys. **5**, 47 (1975).

[31]H. P. Kelly, Adv. Theor. Phys. **2**, 75 (1968); Adv. Chem. Phys. **14**, 129 (1969); in *Photoionization and Other Probes of Many-Electron Interactions,* edited by F. J. Wuilleumier (Plenum, New York, 1976).

[32]C. Pan, S. L. Carter, and H. P. Kelly, J. Phys. B **20**, L335 (1987).

[33]H. P. Kelly and Z. Altun, in *Giant Resonances in Atoms, Molecules, and Solids,* edited by J. P. Connerade, J. M. Esteva,

and R. C. Karnatak (Plenum, New York, 1987).
[34]L. M. Frantz, R. L. Mills, R. G. Newton, and A. M. Sessler, Phys. Rev. Lett. **1**, 340 (1958); B. A. Lippmann, M. H. Mittleman, and K. M. Watson, Phys. Rev. **116**, 920 (1959); R. T. Pu and E. S. Chang, *ibid.* **151**, 31 (1966); H. J. Silverstone and M. L. Yin, J. Chem. Phys. **49**, 2026 (1968); S. Huzinaga and C. Arnau, Phys. Rev. A **1**, 1285 (1970).
[35]U. Fano and J. W. Cooper, Rev. Phys **40**, 441 (1968).
[36]E. R. Brown, S. L. Carter, and H. P. Kelly, Phys. Rev. A **21**, 1237 (1980).
[37]A. F. Starace, in *Korpuskeln and Strahlung in Materie I,* Vol. 31 of *Handbuch der Physik,* edited by W. Mehlhorn (Springer Berlin, 1982), p. 1.
[38]G. E. Brown, *Unified Theory of Nuclear Models and Forces,* 3rd ed. (North Holland, Amsterdam, 1971), pp. 26 and 49; A. L. Fetter and J. D. Walecka, *Quantum Theory of Many-Particle Systems* (McGraw-Hill, New York, 1971), p. 565.
[39]J. Cooper and R. N. Zare, Lect. Theor. Phys. **11C**, 317 (1968).
[40]L. Lipsky, in *Fifth International Conference on the Physics of Electronic and Atomic Collisions; Abstracts of Papers,* edited by V. V. Afrosimov (Nauka, Leningrad, 1967); V. L. Jacobs and P. G. Burke, J. Phys. B **5**, L67 (1972); V. L. Jacobs, *ibid.* **5**, 2257 (1972); D. Dill and U. Fano, Phys. Rev. Lett. **29**, 1203 (1972); U. Fano and D. Dill, Phys. Rev. A **6**, 185 (1972).
[41]This can be clearly seen using the asymptotic form of the final-state wave function including interchannel interactions, e.g., using the expression given in Sec. 4 of Ref. 37.
[42]C. Froese-Fischer, Comput. Phys. Commun. **14**, 145 (1978).
[43]J. P. Desclaux, At. Data Nucl. Data Tables **12**, 311 (1973).
[44]E. J. McGuire, J. Phys. Chem. Solids **33**, 577 (1972).
[45]U. Becker (private communication).
[46]U. Becker, H. G. Kerkhoff, *et al.* (unpublished).